



Published in final edited form as:

Scanning. 2011 September ; 33(5): 342–352. doi:10.1002/sca.20283.

Holographic otoscope for nano-displacement measurements of surfaces under dynamic excitation

J. M. Flores-Moreno^{1,2,6}, Cosme Furlong^{1,2,3,4}, John J. Rosowski^{3,4,5}, Ellery Harrington^{1,2}, Jeffrey T. Cheng^{3,4}, C. Scarpino^{3,4}, and F. Mendoza Santoyo⁶

¹Center for Holographic Studies and Laser micro-mechaTronics, WPI, Worcester, MA, USA

²Department of Mechanical Engineering, WPI, Worcester, MA, USA

³Eaton-Peabody Laboratory, Massachusetts Eye and Ear Infirmary, Boston, MA 02114, USA

⁴Department of Otology and Laryngology, Harvard Medical School, Boston, MA, USA

⁵Speech and Hearing Bioscience and Technology Program, MIT-Harvard Division of Health Sciences and Technology, Cambridge, MA, USA

⁶Centro de Investigaciones en Optica A. C., Leon, Gto, Mexico

Summary

We describe a novel holographic otoscope system for measuring nano-displacements of objects subjected to dynamic excitation. Such measurements are necessary to quantify the mechanical deformation of surfaces in mechanics, acoustics, electronics, biology and many other fields. In particular, we are interested in measuring the sound-induced motion of biological samples, such as an eardrum. Our holographic otoscope system consists of laser illumination delivery (IS), optical head (OH), and image processing computer (IP) systems. The IS delivers the object beam (OB) and the reference beam (RB) to the OH. The backscattered light coming from the object illuminated by the OB interferes with the RB at the camera sensor plane to be digitally recorded as a hologram. The hologram is processed by the IP using Fresnel numerical reconstruction algorithm, where the focal plane can be selected freely. Our holographic otoscope system is currently deployed in a clinic, and is packaged in a custom design. It is mounted in a mechatronic positioning system to increase its maneuverability degrees to be conveniently positioned in front of the object to be measured. We present representative results highlighting the versatility of our system to measure deformations of complex elastic surfaces in the wavelength scale including a copper foil membrane and postmortem tympanic membrane (TM).

Keywords

Optoelectronic holography; digital holography; otology; middle-ear

Introduction

In this paper, we describe a Digital Opto-electronic Holographic system (DOEHO) that we are developing to measure acoustically induced motions of the tympanic membrane (TM) in a non-contact and in full field-of-view mode without the use of magnifying optics. The DOEHO is being designed for use in the clinic and it is complementing the capabilities of

our previously developed holographic system that we are currently using to measure nano-displacements of the TM in laboratory settings (Aarnisalo *et al.* 2010; Cheng *et al.* 2010; Furlong *et al.* 2009; Hernandez-Montes *et al.* 2009; Rosowski *et al.* 2009).

Nano-displacement information of the TM, as key component of the tympano-ossicular system, is used to study how the TM converts environmental sounds to sound pressure and velocity within the inner ear. Deformation measurements with various acoustic stimuli quantify dynamic mobility changes in the entire TM, e.g. before and after a surgical procedure; moreover, helps to determine alterations in the sound transfer to the inner ear when the TM is altered by trauma or middle-ear pathologies that results in conductive hearing loss capabilities. Additionally, motion measurements of the entire TM surface in response to sound, as obtained with our DOEHO, could be used to resolve other issues, such as the nature of TM function at higher frequencies and the hypothesized presence of standing or travelling surface waves on the surface of the TM (Aarnisalo *et al.* 2010; Furlong *et al.* 2009; Rosowski *et al.* 2009).

Our DOEHO system utilizes the two conventional steps needed to recover intensity and phase information in holography: recording and reconstruction (Furlong and Pryputniewicz 1998; Hariharan *et al.* 1987b; Pryputniewicz and Stetson 1989; Stetson and Brohinsky 1987; Vest C. 1979). Recording is done by a digital camera and reconstruction is performed numerically by a computer. Numerical reconstruction is based on diffraction by Fresnel approximation with phase shifting, which enables a compact lensless interferometric configuration that is suitable for use in the clinic. In addition, numerical reconstruction allows focusing by software after holographic data have been recorded (Schnars and Juptner 2005). All of these characteristics have allowed the development of the holographic system for measurements in the clinic.

The DOEHO consists of a laser illumination delivery (IS) system, optical head (OH) system that includes a sound presentation subsystem (SPS), and image processing computer (IP) system. In addition, the packaged OH is attached onto a mechatronic positioning subsystem with sufficient degrees of freedom for an examiner to easily place the OH at the right working distance to quantitatively measure acoustically induce motions of the TM.

Methods

The basic DOEHO setup is shown in Fig. 1. The system consists of four main components: the IS system that provides the coherent illumination; the OH system that superimposes backscattered light from the object with the reference illumination at the sensor camera plane; the IP system that supplies the electronic signals required to perform phase-shifting and displays the numerical reconstruction of the digitally recorded holograms at video rates; and the positioning system (PS). The OH system includes the SPS to deliver controlled sound excitation to the sample. In addition to these modules, the OH is custom packaged onto the mechatronic PS, which helps to position the OH near the TM while maintaining its relative orientation during measurements.

Laser illumination delivery system

The IS system, as shown in Fig. 2, consists of a Coherent Compass 315M solid-state laser (LR) with a wavelength of 532 nm and a power of 50 mW to deliver as much intensity illumination as possible on the OH side; a Gooch & Housego 23080-1-LTD acousto-optic modulator (AOM) at the frequency of 110 MHz for stroboscopic illumination; an 80:20 beam splitter cube (BS) to divide the laser light into two beams; two New Focus fiber optic assemblies (FA) to couple the divided beams into polarization maintaining fibers (PM); one Physik Instrumente P-830.10 piezoelectric nanopositioner (PZ) with steering mirror (M2)

for phase shifting; and two mechanical shutters for beam blocking and measurement of reference-object beam ratio.

According to Fig. 2, the collimated LR passes through the AOM and the BS cube, which divides the input beam into 80% for object beam (OB) and 20% for reference beam (RB). OB is steered to one of the FA by means of mirror (M1) while RB is steered to the second FA by means of mirror (M2) which is attached onto the PZ that introduces $\pi/2$ phase shifts. Both of the FA's are FC connectorized.

Optical head system

Design of the optical head—The TM is a thin, virtually transparent and delicate soft tissue composed mainly of collagen fibers. Its geometry is characterized by a cone-like shape with an apex angle of approximately 120° , diameter on the order of 7mm , and depth of 2mm (Decraemer and Funnell 2008). We considered the anatomic characteristics of the TM to define the design parameters of the OH system.

The OH is arranged in an in-line lensless holographic setup that enabled the realization of a compact opto-mechanical configuration, as depicted in Fig. 3. In this configuration, the RB and the backscattered light from the object are directed normal to the camera by the use of a beam splitter cube. The anatomic characteristics of the TM, such as size and dimensions, constrained the optoelectronic characteristics of the design, including depth of field, TM reflectivity, lateral resolution, region of interest (ROI), camera acquisition speed, and the working distance between OH and the sample.

Realization of the optical head—To define the opto-mechanical configuration of the OH we utilized an otoscope, which is a standard tool used in the otology clinic. The otoscope already has the characteristics that are necessary for observation of the TM together with illumination capabilities. In addition to the otoscope, the OH is further defined by a beam splitter cube that acts as a beam combiner and a CCD camera for holographic recordings. Capabilities for acoustic excitation of the TM and monitoring of the applied sound characteristics are provided by a custom designed SPS (Bapat 2011), which contains a miniaturized speaker and a microphone embedded on a package attached to the otoscope head. RB and OB, as shown in Fig. 3, are provided by the IS.

To be able to measure nano-scale displacements of the entire TM, the components of the OH are arranged in an optical configuration capable of providing sufficient measuring and lateral resolutions as well as a depth of field (DOF) that are consistent with the anatomical characteristics of the TM. In addition, we selected a working distance, defined as the distance between the tip of the otoscope and the TM, of 30mm , which is the distance commonly used by clinicians.

The specific equipment used in the OH, includes a 25020 Diagnostic fiber optic Welch Allyn, an AVT Pike F-100B digital camera running at 60 fps at the full resolution of 1000×1000 , bit depth of 8–16 bits, and a pixel size of $7.4 \times 7.4 \mu\text{m}^2$, and a non-polarized 50-50 BS cube coated for visible range.

The combination of the optical arrangement and the hardware used allow achieving a 100% pixel fill factor and the capability to observe the entire TM with a Region of Interest (ROI) of 800×800 pixels at the magnification of 0.85. With the lensless in-line DH configuration, image focusing is done numerically by software and, therefore, avoiding any mechanical adjustments. The custom packaged design is shown in Fig. 4, where the SPS is included. This package includes fixtures that allow attachment of the OH onto the positioning system of the DOEHO.

Testing of the optical head—The optical characteristics of the OH were measured experimentally by a standard USAF target and 5–15 DOF target from Edmund Optics. At the designed working distance of 30 mm, the field of view (FOV) was measured by imaging line-pair patterns on the targets, which resulted in a FOV of 7 mm and a DOF of 6 mm.

The spatial resolution of the OH was measured in terms of the Modulation Transfer Function (MTF) using the USAF target, as shown in Fig. 5. The dotted line represents the fitting curve of the experimental data depicted by the continuous line. Because of the use of a coherent light source, speckles reduce the spatial resolution of the reconstructed image. Other aspects that affect the spatial resolution of numerically reconstructed images have been reported by Goodman (2005), Kreis (2005), Schnars and Juptner (2005) and Yamaguchi *et al.* (1997).

Computer processing subsystem—The IP subsystem is used to perform multiple tasks including processing of images recorded by the camera in the OH, display of image data in the form of interferometric or optical phase measurements, control of the electronic signals used for sample loading and for focusing of the reconstructed image. The IP uses a series of concurrent threads to acquire images, control the hardware, and display quantitative holographic data at video rates. The IP connects to the camera via a Firewire connection to capture a video stream directly from the camera while synchronizing image capture with the optical-phase steps of the PZ (Harrington *et al.* 2010). The IP uses a data acquisition board to vary the analog voltage that controls the PZ and the mechanical shutters. Phase-stepped images are acquired by triggering the PZ immediately after the camera's integration of the previous image is complete.

Positioning system—The positioning system (PS) is a mechatronic configuration capable of locating the holographic otoscope at the patient's ear while maintaining its relative orientation during examinations. The system is guided by the examiner, but maintains the chosen position automatically. For simplification, the mechanism contains no actuators, but only adjustable friction elements in a haptic feedback control system. This renders the positioning system safe and easily applicable to current examination rooms (Dobrev *et al.* 2010).

Theoretical analysis

Computation of holograms in time-averaged (TA) mode

Optical phase measurements are based on phase-stepping algorithms. The camera acquires four successive interference data images in steps of one quarter of a wavelength (Rosowski *et al.* 2009). Thus the intensity distribution of the n -th frame can be expressed as

$$I_n(x, y) = I_o(x, y) + I_r(x, y) 2 \sqrt{I_o(x, y) I_r(x, y)} \cos[\Delta\phi(x, y) + \alpha_n] M[\Omega(x, y)] \quad (1)$$

where $n = 1, 2, 3, 4$ and $M[\Omega(x, y)]$ is the known characteristic function of the time-average

integral determined by the temporal motion of the object under study and $\alpha_n = 0, \frac{\pi}{2}, \pi, \frac{3\pi}{2}$ is the optical phase change.

The modulation intensity from Eq. 1 is evaluated by

$$I_M(x, y) = \sqrt{[I_1(x, y) - I_3(x, y)]^2 + [I_2(x, y) - I_4(x, y)]^2}. \quad (2)$$

Specifically the corresponding fringe pattern intensity at each position (x, y) of the image is modulated, for parallel illumination-observation conditions, by the square of the zero order Bessel function of the first kind as (Pryputniewicz 1999),

$$I_M(x, y) \sim I_0 \left[J_0 \left[\frac{4\pi}{\lambda} d_z(x, y) \right] \right]^2, \quad (3)$$

thus, for non-trivial values of the measured light intensity, centers of the dark fringes are located at those points on the object surface where J_0^2 equals zero.

Computation of the holograms with stroboscopic holographic interferometry

In stroboscopic double-exposure (ST) holographic interferometry the deformations of the object are measured with respect to a reference stage, where the object is not subject to any controlled external excitation signal (Cheng *et al.* 2009). Two sets of stepped images must be acquired since the measurements have to be recorded at two different states. The result of this variation in the movement of the object with respect to its initial position is the observation of the cosine fringe patterns. In the stroboscopic mode the AOM is frequency locked to the external stimulus that deform the TM sample while the phase of the stroboscopic pulses are controlled to illuminate the sample at different locations on the vibration cycle. The resultant modulation intensity distribution corresponding to the difference between two vibration states is calculated with

$$I_M = \sqrt{(I_1 - I_3 + I_{R1} - I_{R3})^2 + (I_2 - I_4 + I_{R2} - I_{R4})^2}, \quad (4)$$

where $I_{R1}, I_{R2}, I_{R3}, I_{R4}$ are the reference state phase-stepped images and I_1, I_2, I_3, I_4 are the deformed state phase-stepped images.

The optical phase difference, $\Delta\phi$, that describes the relative displacement between two vibration states is

$$\Delta\phi = \tan^{-1} \left[\frac{(I_1 - I_3)(I_{R2} - I_{R4}) - (I_2 - I_4)(I_{R1} - I_{R3})}{(I_1 - I_2)(I_{R2} - I_{R4}) + (I_2 - I_4)(I_{R2} - I_{R4})} \right]. \quad (5)$$

This optical phase difference is wrapped modulo $[-\pi, +\pi]$ and needs to be unwrapped to remove the phase ambiguities (Harrington *et al.* 2011).

Phase-shifting digital holography

In the DOEHO system, phase-shifting digital holography is used to reconstruct intensity and phase information at the image plane from the backscattered light modulated by the object that is recorded at the CCD plane. Because of the opto-mechanical geometry of the OH, numerical reconstruction by Fresnel approximation is used, which is derived from the Huygens-Fresnel principle and is valid when the distance between the detector of the CCD and the object, d , satisfies (Goodman 2005)

$$d^3 \gg \frac{\pi}{4\lambda} [(x - \xi)^2 + (y - \eta)^2]^2, \quad (6)$$

where (x, y) are the object plane coordinates, (ξ, η) are the CCD coordinates, and λ is the wavelength of the laser used. The discrete version of the Fresnel approximation is

implemented by Fast-Fourier-Transform (FFT) algorithms, which allow the recovery of intensity and phase at video rates. In addition, FFT implementations enable the selection of specific reconstruction distances and, therefore, image focusing without the need of mechanical elements.

After acquiring phase-stepped images in either TA or ST mode, intensity and phase information are recover from the numerically reconstructed complex amplitude distribution at any selected image plane with

$$I'(x', y') = |b'(x', y')|^2 \tag{7}$$

$$\varphi'(x', y') = \tan^{-1} \left[\frac{\text{Im} |b'(x', y')|}{\text{Re} |b'(x', y')|} \right], \tag{8}$$

where (x', y') are the image plane coordinates, $b'(x', y')$ is the complex reconstructed wavefront obtained by the Fresnel approximation, and $I'(x', y')$ and $\varphi'(x', y')$ are the intensity and optical phase at the image plane, correspondingly. Holograms are recorded by synchronizing image acquisition and phase-stepping with each phase-step introduced by one of the calibrated PZ's of the IS system (Hariharan *et al.* 1987a).

Figure 6 depicts the recording and reconstruction geometry as well as the image focusing capabilities of our implemented algorithms.

According to the geometry shown in Fig. 6, the Fresnel reconstruction algorithm in the image plane located at the distance d' is (Kreis 2005; Schnars and Juptner 2005)

$$b'(x', y') = \frac{\exp(ikd')}{i\lambda d'} \exp \left[i \frac{\pi}{\lambda d'} (x'^2 + y'^2) \right] \times \int_{-\infty}^{\infty} \int_{-\infty}^{\infty} U(\xi, \eta) r^*(\xi, \eta) \exp \left[i \frac{\pi}{\lambda d'} (\xi^2 + \eta^2) \right] \exp \left[-i \frac{2\pi}{\lambda d'} (x' \xi + y' \eta) \right] d\xi d\eta, \tag{9}$$

where d is the recording distance, d' is the reconstruction distance, $U(\xi, \eta)$ is the complex amplitude at the recording plane computed with

$$U(\xi, \eta) = (I_1 - I_3) + i(I_4 - I_2), \tag{10}$$

$r^*(\xi, \eta)$ (is the complex amplitude distribution of the reference wave required for reconstruction of the real image, where * indicates complex conjugated, with the quadratic phase term inside the double integral representing the broadening of the reconstruction wavefront. Accuracy of Eq. 9 is based on the fundamental assumption that the distances d and d' are larger than the maximum dimensions of the CCD detector (Goodman 2005, Kreis 2005, Schnars and Juptner 2005). The first exponential term to the right of the equal sign in Eq. 9 represents a constant phase delay and the second exponential term before the double integral is a multiplicative constant applied when the continuous integral is discretized. Therefore, the discrete form of Eq. 9 is represented as

$$b'(m, n) = \text{const} \exp \left[i\pi\lambda d' \left(\frac{m^2}{M^2\Delta\xi^2} + \frac{n^2}{N^2\Delta\eta^2} \right) \right] \times \sum_{k=0}^{N-1} \sum_{l=0}^{N-1} U(k\Delta\xi, l\Delta\eta) r^*(k\Delta\xi, l\Delta\eta) \exp \left[i \frac{\pi}{\lambda d'} (k^2\Delta\xi^2 + l^2\Delta\eta^2) \right] \exp \left[-2\pi \left(\frac{km}{M} + \frac{ln}{N} \right) \right]. \tag{11}$$

In Eq. 11, $(M \times N)$ are the number of pixels and $\Delta\xi$ and $\Delta\eta$ are the pixel sizes of the CCD detector with $\Delta x' = \lambda d' / M \Delta\xi$ and $\Delta y' = \lambda d' / N \Delta\eta$ defining the spatial resolution in the image plane. Accordingly, spatial resolution is limited by the wavelength, the reconstruction distance, the characteristics of the CCD detector, as well as the dimensions of the objective speckle (Goodman 2005).

Experimental results

System validation

Before applying our DOEHO system to characterized nano-displacements of the TM, we first proceeded to investigate a mechanical system subjected to well control boundary conditions and known mechanical properties. Such a system was defined by a circular 110 copper alloy foil membrane having a thickness of 0.0155mm and a diameter of 6mm .

The membrane was fabricated by cutting a circular piece of copper foil sheet while making sure that residual stresses were minimized. The membrane was mounted by the edge on a custom designed aluminum ring stage, which guaranteed fixed boundaries conditions. The membrane was acoustically excited with the SPS in a range of frequencies between 0.5 and 17kHz . The DOEHO was set to the designed magnification of 0.85 , a FOV on the order of 7mm , and a ROI of $800 \times 800\text{ pixels}$. To maximize fringe visibility the beam ratio, RB/OB , was set to 1.5 (Hernandez-Montes *et al.* 2009).

Measurements in TA mode of the circular 110 copper alloy foil membrane

The fundamental modes of vibration were first identified with the DOEHO set in TA mode. Figure 7 shows the first four resonant modes of vibration of the 110 copper foil alloy membrane, as recorded and numerically reconstructed at video rates. The identified modes of vibration correspond to the frequencies of 2.774 , 6.166 , 10.176 , and 15.187 kHz .

Measurements in ST mode of the circular 110 copper alloy foil membrane

The identified modes of vibration of the 110 copper alloy foil membrane were quantified with the DOEHO set in ST mode. Digital holograms were acquired by synchronizing the stroboscopic pulses with the deformations produced by acoustic excitation provided by the SPS. Recorded holograms were processed to extract optical phase information corresponding to the deformation patterns, as is shown in Figs. 8a)–c).

To illustrate our analyses procedures, we proceeded to quantify the deformations of the third resonance mode of vibration, which corresponds to the frequency of 10.1276 kHz with the TA mode shown in Fig. 7c). Same quantification steps were applied to the other identified modes of vibration. Figures 8a) and 8b) show the module 2π wrapped optical phase and the unwrapped phase of the selected frequency, correspondingly. Measurements indicate a difference between maximum and minimum deformations of $1110 \pm 20\text{nm}$ at a specific excitation level, as is depicted in Fig. 8c), which can be modified to study different loading conditions.

The results of the measured and computed unwrapped phase were compared with predictions obtained with equivalent analytic models and computer simulations by finite element analysis (FEA). For the simulations we used COMSOL-Multiphysics software to found the vibrations modes on the copper foil membrane using the structural and eigenvalues modules, corresponding to its natural frequencies. In the model, tetrahedral elements were used. The number of elements was defined based on the convergence of the solution on different mesh sizes (Bapat, 2011). In our case, the convergence is reached with 27371 elements and 273710 nodes.

Table I shows comparisons between experimental, analytical (Leissa 1969; Reddy 1999; Hulli, 2008), and computational results, demonstrating excellent agreement and validating the system to characterized nano-displacements of the TM. The difference between FEA and analytical solution basically corresponds to the uncertainty on the parameters selected in the simulation more specifically the exact material properties as well the accuracy of the boundary conditions.

Measurements of TM

After validation of the DOEHO, we proceed to investigate deformations of cadaveric chinchilla TM while acoustically stimulated. The eardrum was prepared by drilling away the bony external ear canal leaving wide open the TM and then was lightly painted with a solution of TiO_2 powder in saline to increase the amount of light reflected from it (Rosowski *et al.* 2009).

First we proceeded to identify the modes of vibration of the sample by setting the DOEHO in TA mode as it was the case with the copper alloy foil membrane. The acoustic excitation was delivered with the SPS in the hearing frequency range of 20Hz to 25kHz . Figure 9 shows reconstructed TA holograms corresponding to the identified frequencies of 0.776 , 1.085 , 3.489 and 7.675 kHz .

Quantification of TM deformations of the identified modes of vibrations was done by setting the DOEHO in ST mode, describing the differences in optical phase between two stimulus phases corresponding to absolute deformations with nanometer resolution. In order to illustrate our measurement procedures, Figs. 10a) and 10b) show module 2π optical wrapped and unwrapped phase corresponding to the identified mode of vibration of 3.489kHz , depicted in Fig. 9c). Sample stability is an issue when doing measurements in ST mode. In order to minimize the effects of the external disturbances onto the sample, the duration of the stroboscopic pulses is set smaller than the period of the excitation signal, which is achieved by controlling the duty cycle of the stroboscopic pulses used in the AOM. In some of our measurements we have used duty cycles as small as 1%. One of the features of our digital holographic software includes the capability to record holographic data while the phase of the stroboscopic illumination is set at different locations relative to the excitation signal. Figure 10 shows analysis of ST holograms recorded with the stroboscopic pulse set at 45 degrees offset with respect to the beginning of the excitation signal. In Fig. 10c) peak-to-peak deformations on the order of 800 nm are shown. Since the measurements are obtained using an interferometric technique, in our system the minimum quantifiable deformation is around $\lambda/20$. In our case, the last two significant figures are highly dependent of the noise level in the recorded intensity images affecting the spatial resolution of the numerically reconstructed images (Goodman 2005; Kreis 2005; Schnars and Juptner 2005; Yamaguchi *et al.* 1997).

Measurements in ST mode demonstrate the DOEHO system's ability to describe differences in optical phase of a deformed state with respect to its undeformed state and to convert those differences into absolute displacements of the entire reconstructed image. Understanding the significance of the measured vibration patterns of the TM is an ongoing task for otologists and for hearing researchers, who can use such data to further investigate the biomechanics of the hearing process as well as to diagnose changes in TM mobility when affected by middle-ear diseases.

In addition, these measurements could help to study the viscoelastic properties and other mechanical properties used for finite element (FE) modeling of the TM. In the literature, most of the FE modeling used to study mechanical properties of the TM is done assuming a homogenous and isotropic model (Cheng *et al.* 2006; Fay *et al.* 2006). However, there is

some evidence suggesting that models that consider anisotropic arrangements of collagen fibers in the TM show improved high-frequency response (O'Connor *et al.* 2008).

Conclusions

We have described a digital optoelectronic holographic otoscope (DOEHO) system capable of providing qualitative and quantitative information of deformations in surfaces subjected to controlled acoustic excitation in a full-field-of-view and non-contact mode with nanometer resolution at video rates. With the implementation of numerical reconstruction algorithms based on diffraction by Fresnel approximation, the focusing can be freely adjusted both during and after the recording avoiding the use of lenses to form an image. The DOEHO includes an imaging-processing computer system to display and process the information of digitally recorded holograms. The optical head system is custom packaged and attached to a positioning system, resulting in a maneuverable apparatus that can be placed at the vicinity of an object of interest, e.g., the eardrum of the middle-ear. Image quality and resolution were evaluated using standard test samples. To further illustrate the measurement capabilities of the DOEHO system, we measured the fundamental vibrations modes of a copper foil membrane and compared them with the predicted modes obtained by analytical solutions and computer simulations (FEA). Finally, we showed representative results of a post-mortem chinchilla TM acoustically excited, which are in agreement with our recent reported data. The system is currently being used to continue our clinical research conducted to study TM. The DOEHO is a tool that can effectively be applied to investigate objects in confined volumes subjected to different types of loading conditions. Our current efforts are aimed at bringing the DOEHO to the otology clinic.

Acknowledgments

This research was supported by the U.S. National Institute for Deafness and other Communicative Disorders (NIDCD). Partial support provided by Worcester Polytechnic Institute (WPI), Centro de Investigaciones en Óptica, A. C. (CIO), Massachusetts Eye and Ear Infirmary (MEEI), and the Lakshmi Mittal fund. We would also like to acknowledge the support of our collaborators at the WPI-ME/CHSLT laboratories and the MEEI.

References

- Aarnisalo AA, Cheng JT, Ravicz ME, Furlong C, Merchant SN, Rosowski JJ. Motion of the tympanic membrane after cartilage Tympanoplasty determined by stroboscopy holography. *Hear Res.* 2010; 263:78–84. [PubMed: 19909803]
- Bapat, N. Master of Science Thesis. Mechanical Engineering Department, Worcester Polytechnic Institute; 2011. Development of Sound Presentation System (SPS) for Characterization of Sound Induced Displacements in Tympanic Membranes.
- Cheng JT, Aarnisalo AA, Harrington E, Hernandez-Montes MdS, Furlong C, Merchant SN, Rosowski JJ. Motion of the surface of the human tympanic membrane measured with stroboscopic holography. *Hear Res.* 2010; 263:66–77. [PubMed: 20034549]
- Cheng JT, Dai C, Gan RZ. Viscoelastic properties of human tympanic membrane. *Ann Biom Eng.* 2006; 35:305–314.
- Decraemer, W.; Funnell, W. Chronic otitis media. Pathogenesis-oriented therapeutic management. 2008. Anatomical and mechanical properties of the tympanic membrane; p. 51-84.
- Dobrev, I.; Flores-Moreno, JM.; Furlong, C.; Harrington, EJ.; Rosowski, JJ.; Scarpino, C. Design of a positioning system for a holographic otoscope. *Proceedings of SPIE*; Sn. Diego, CA. 2010. p. D1-D12.
- Fay JP, Puria S, Steele CR. The discordant eardrum. *PNAS.* 2006; 103:19743–19748. [PubMed: 17170142]
- Furlong C, Pryputniewicz RJ. Hybrid computational and experimental approach for the study and optimization of mechanical components. *Opt Eng.* 1998; 37:1448–1455.

- Furlong C, Pryputniewicz RJ. Optoelectronic characterization of shape and deformation of MEMS accelerometers used in transportation applications. *Opt Eng.* 2003; 42:1223–1231.
- Furlong C, Rosowski JJ, Hulli N, Ravicz ME. Preliminary Analyses of Tympanic-Membrane Motion from Holographic Measurements. *Strain.* 2009; 45:301–309. [PubMed: 20209120]
- Goodman, JW. Introduction to Fourier optics. 3rd ed. Roberts&Company; 2005.
- Hariharan P, Oreb BF, Eiju T. Digital phase-shifting interferometry: a simple error-compensating phase calculation algorithm. *App Opt.* 1987a; 26:2504–2505.
- Hariharan P, Oreb BF, Freund CH. Stroboscopic holographic interferometry: measurements of vector components of vibration. *Appl Opt.* 1987b; 26:3899–3903. [PubMed: 20490160]
- Harrington, E.; Dobrev, I.; Bapat, N.; Flores, JM.; Furlong, C.; Rosowski, JJ.; Cheng, JT.; Scarpino, C.; Ravicz, M. Development of an optoelectronic holographic platform for otolaryngology applications. *Proceedings of SPIE; San Diego, CA.* 2010. p. J1-J14.
- Harrington, E.; Furlong, C.; Rosowski, JJ.; Cheng, JT.; Flores, JM.; Lu, W.; Dobrev, I. Automatic Acquisition and Processing of Large Sets of Holographic Measurements in Medical Research. *Proceedings of SEM; Uncasville, CT.* 2011.
- Hernandez-Montes, Mds; Furlong, C.; Rosowski, JJ.; Hulli, N.; Harrington, E.; Cheng, JT.; Ravicz, ME.; Mendoza, SF. Optoelectronic holographic otoscope for measurement of nano-displacements in tympanic membranes. *J Biomed Opt.* 2009; 14:034023. [PubMed: 19566316]
- Hulli, N. Master of Science Thesis. Mechanical Engineering Department, Worcester Polytechnic Institute; 2008. Development of an optoelectronic holographic otoscope system for characterization of sound-induced displacements in tympanic membranes.
- Kim M. Principles and techniques of digital holographic microscopy. *SPIE Rev.* 2010; 1:2–50.
- Kreis, T. Handbook of Holographic Interferometry. Wiley-VCH GmbH&Co. KGaA; 2005.
- Leissa, AW. Vibration of Plates. Vol. 160. NASA SP; 1969.
- O'Connor KN, Tam M, Blevins NH, Puria S. Tympanic membrane collagen fibers: a key to high-frequency sound conduction. *Laryngoscope.* 2008; 118:483–490. [PubMed: 18091335]
- Pryputniewicz, RJ.; Stetson, KA. Measurement of vibration patterns using electro-optic holography; *Proceedings of SPIE;* 1989. p. 456-467.
- Pryputniewicz, RJ. Holographic numerical analysis. Worcester, MA: Worcester Polytechnic Institute, Department of Mechanical Engineering; 1999.
- Reddy, JN. Theory and analysis of elastic plates. Taylor & Francis; 1999.
- Rosowski JJ, Cheng JT, Ravicz ME, Hulli N, Hernandez-Montes MdS, Harrington E, Furlong C. Computer-assisted time-averaged holograms of the motion of the surface on the mammalian tympanic membrane with sound stimuli of 0.4–25kHz. *Hear Res.* 2009; 253:83–96. [PubMed: 19328841]
- Schnars, U.; Juptner, W. Digital Holography. Springer-Verlag; 2005.
- Stetson KA, Brohinsky WR. Electro-optic holography system for vibration analysis and nondestructive testing. *Opt Eng.* 1987; 26:1234–1239.
- Takeda, M.; Taniguchi, K.; Hirayama, T.; Kohgo, H. Simulation and Experiment in Laser Metrology. Berlin: Akademie Verlag; 1996. Single-Transform Fourier/Hartley fringe analysis for Holographic Interferometry.
- Yamaguchi I, Zhang T. Phase-shifting digital holography. *Opt Lett.* 1997; 22:1268–1270. [PubMed: 18185816]
- Yamaguchi I, Kato J, Matsuzaki H. Measurement of surface shape and deformation by phase-shifting image digital holography. *Opt. Eng.* 2003; 42:1267–1271.
- Vest, C. Holographic Interferometry. New York: John Wiley & Sons Inc.; 1979.

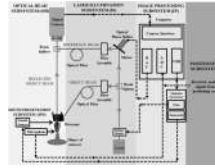


Fig 1.
DOEHO setup depicting major systems and control signals.

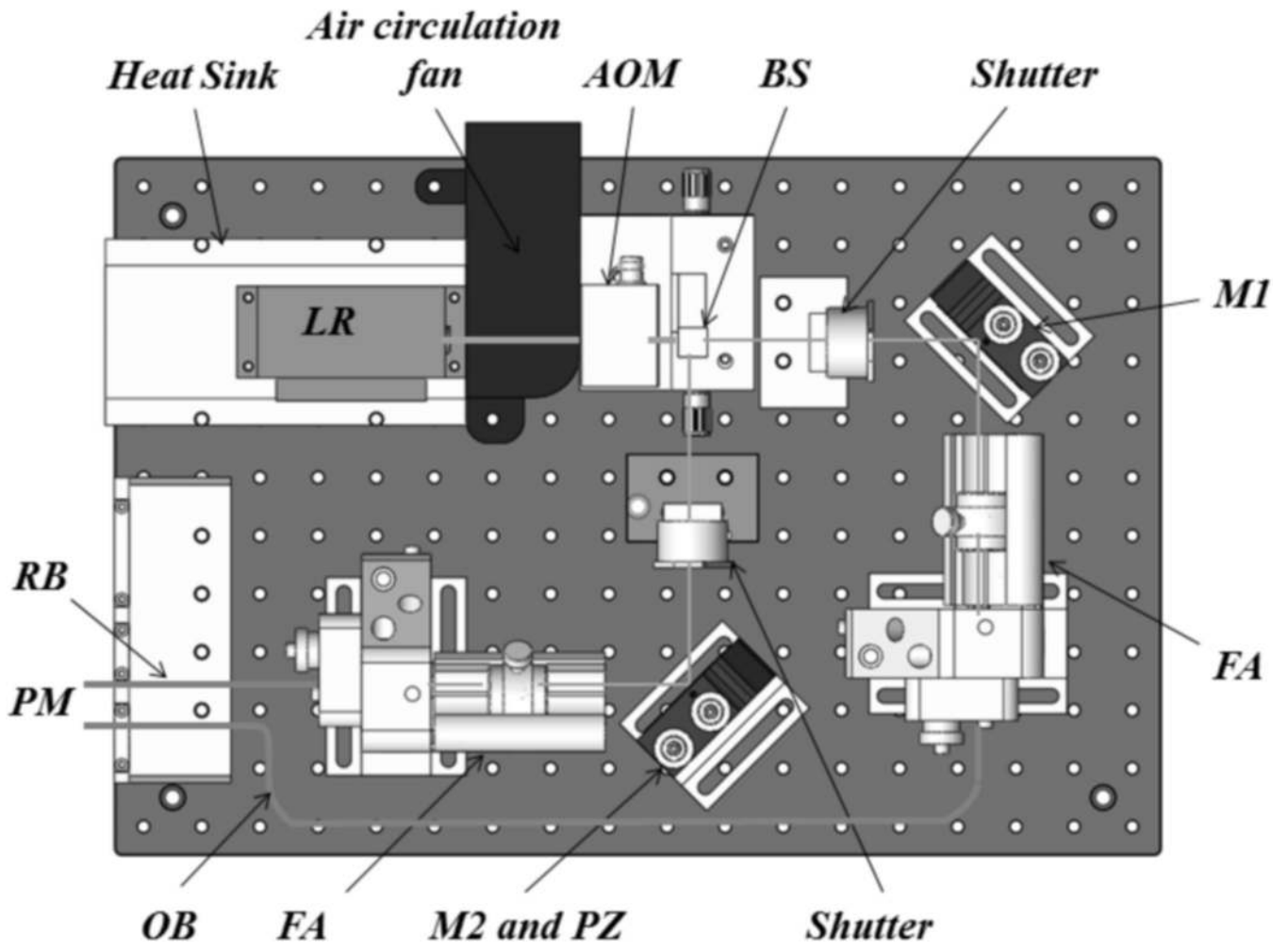


Fig 2.
Schematic of the laser delivery system of the DOEHO.

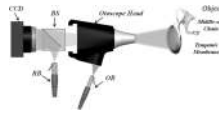


Fig 3.
In-line holographic configuration of the OH of the DOEHO.

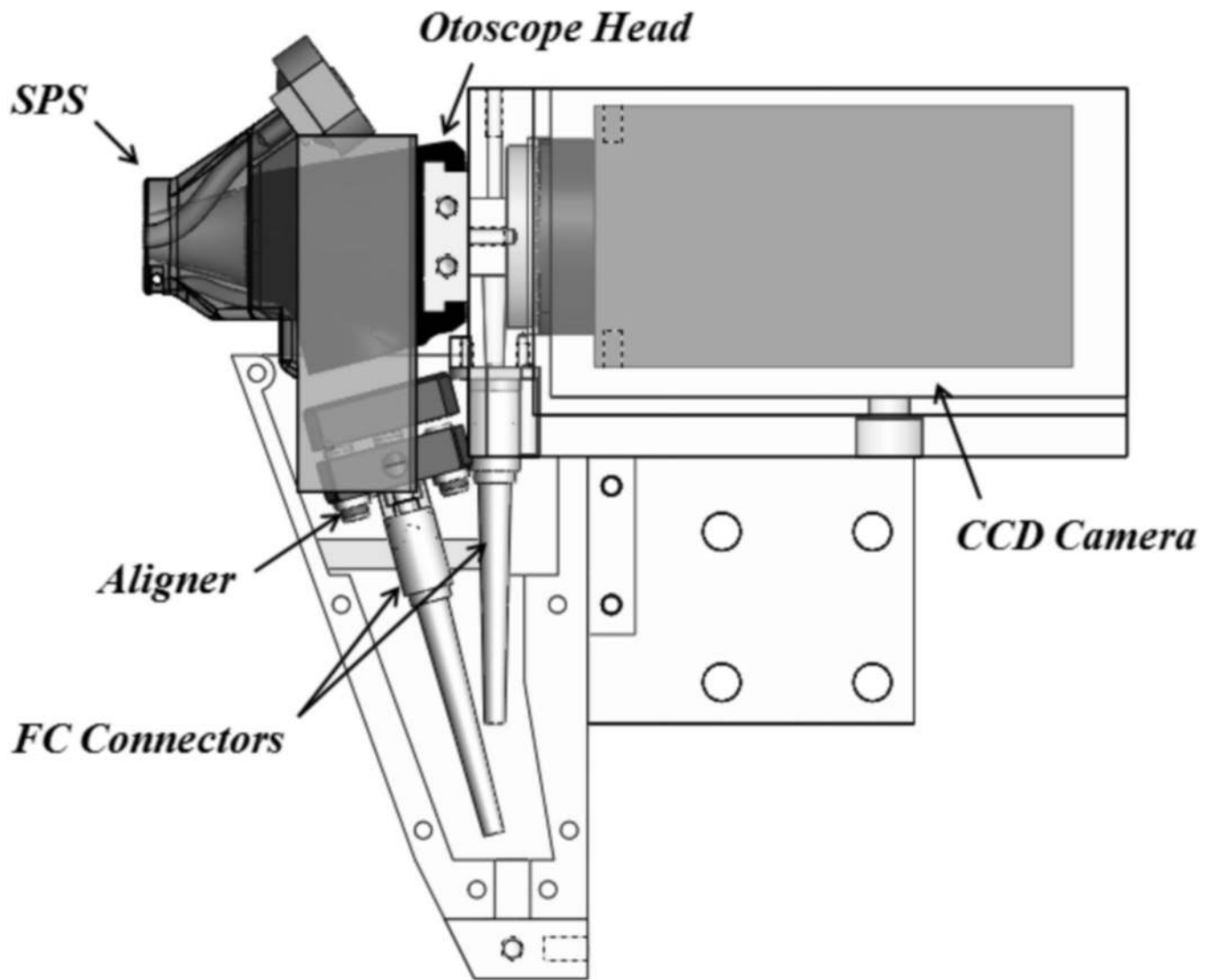


Fig 4. Design of the custom packaged OH and the SPS (FC, fiber couplers).

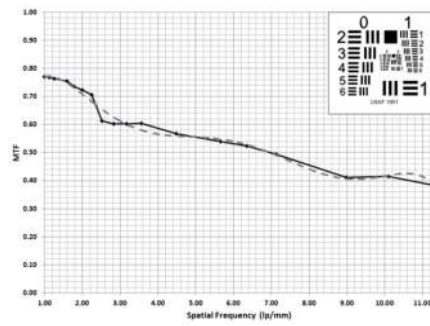


Fig 5. MTF chart measured using a USAF target, shown in the graph. The dotted line represents the fitting curve of the experimental data depicted by the continuous line.

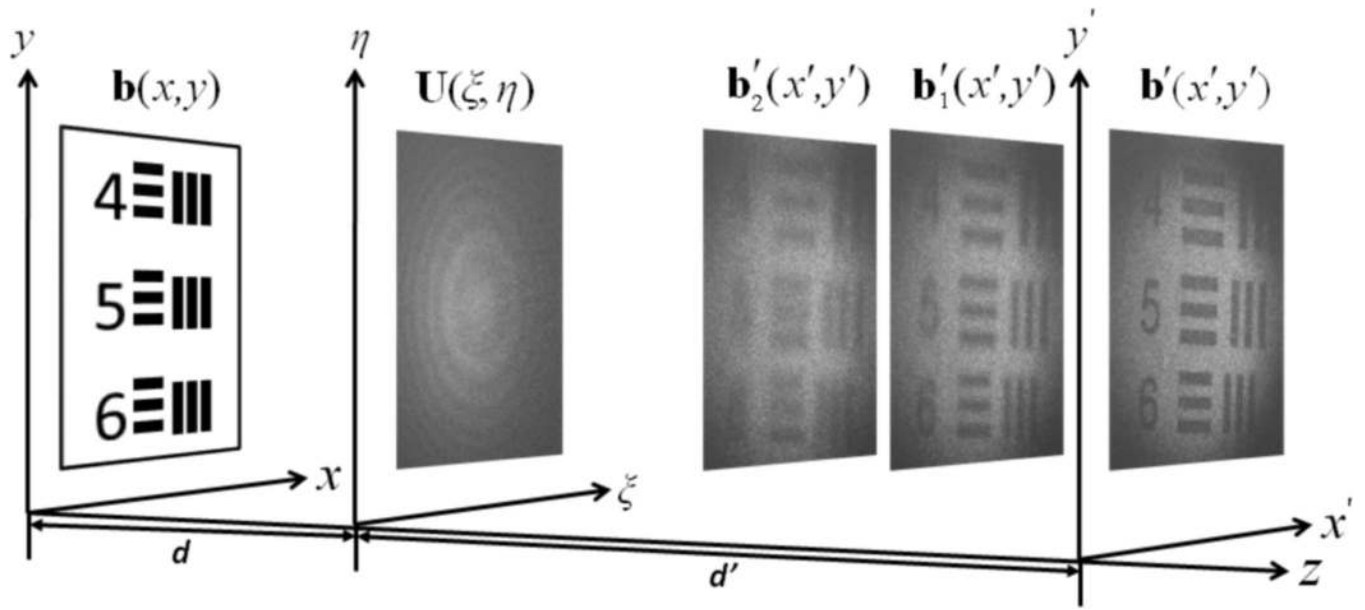


Fig 6. Recording and reconstruction geometry showing reconstructed wavefronts, $b'(x', y')$, at successive distances d' .

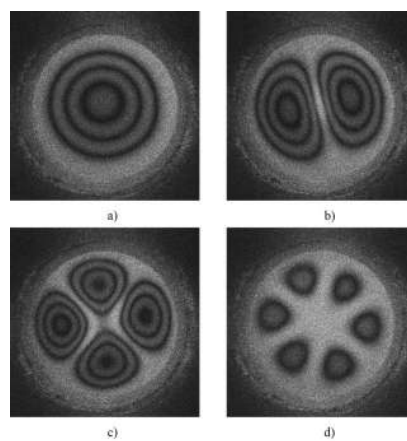


Fig 7. Fundamental modes of vibration of the copper foil membrane obtained with the DOEHO in TA mode: a) 2.774 kHz, b) 6.166 kHz, c) 10.176 kHz, and d) 15.187 kHz.

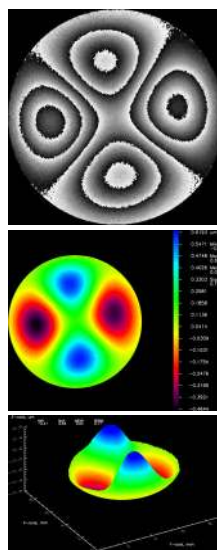


Fig 8.

Fig 8a). Wrapped phase map corresponding to the deformations of the copper foil membrane acoustically excited at the frequency of 10.1276 kHz .

Fig 8b). Unwrapped phase map corresponding to Fig. 8a). Observation of the entire perimeter of the membrane is limited by the optical aperture defined by the otoscope tip.

Fig 8c). 3D deformations corresponding to Fig. 8b) showing a peak-to-peak out-of-plane deformation, d_z , of 1110 nm .

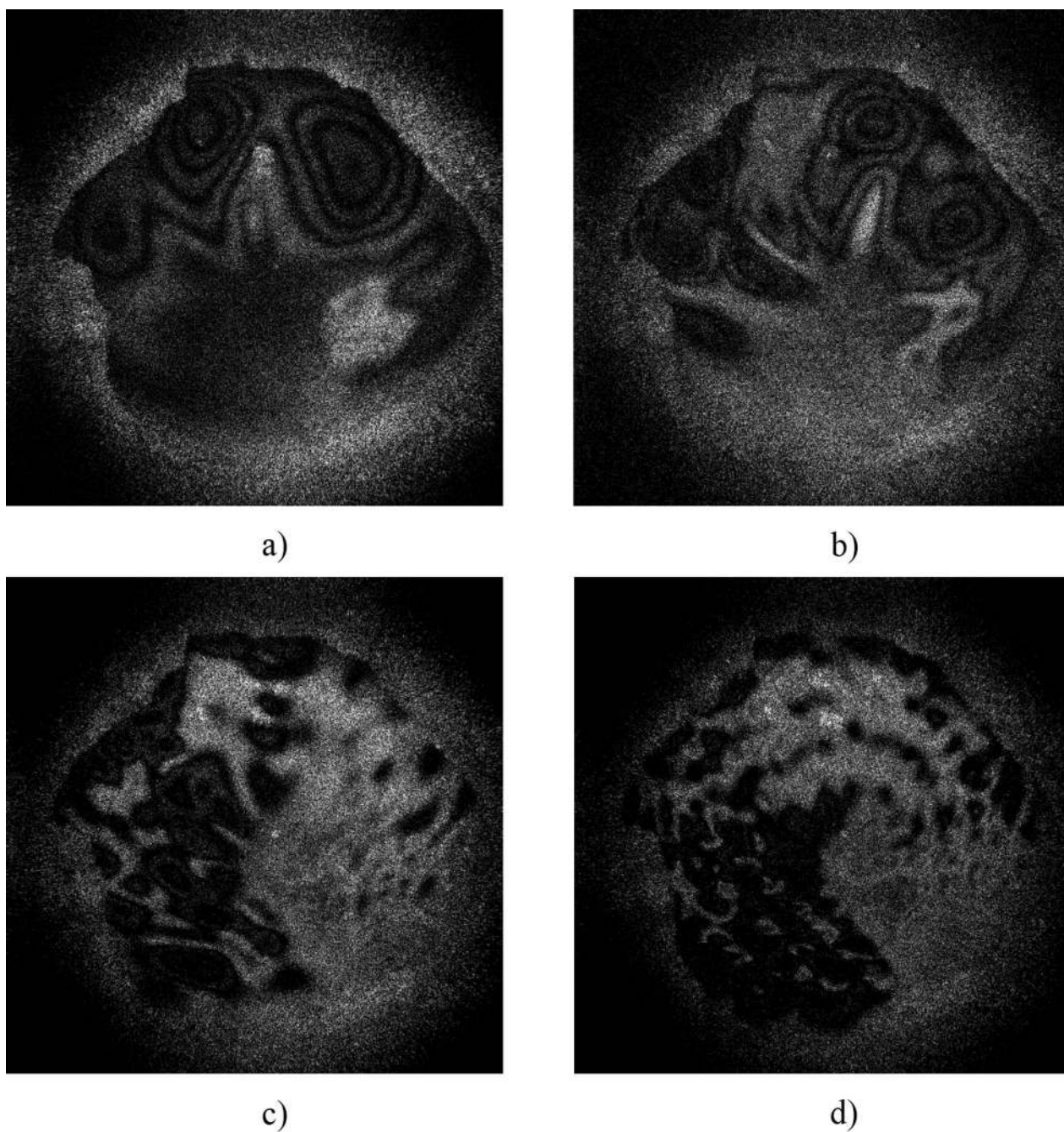
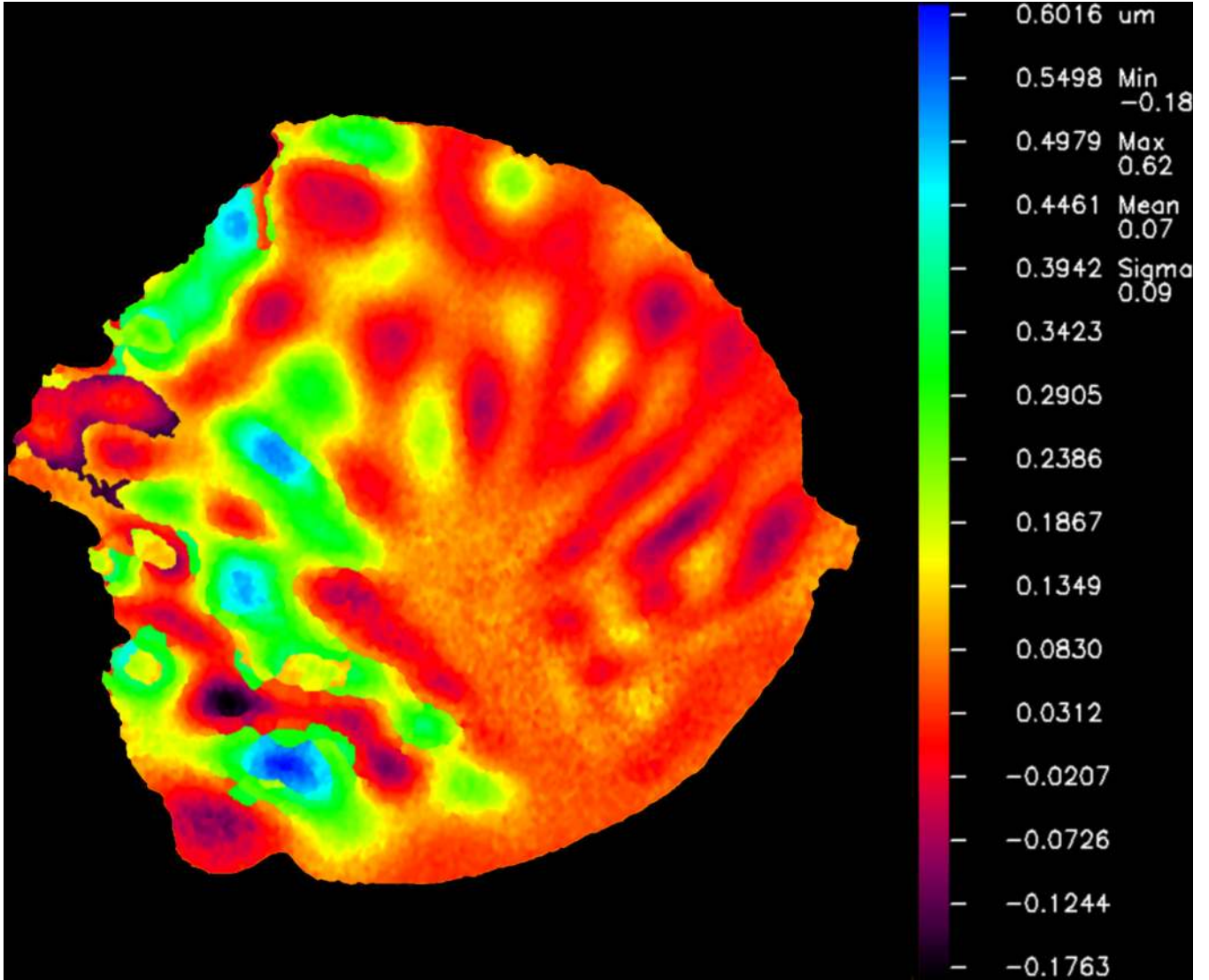
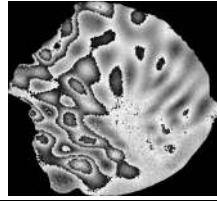


Fig 9. Time-average modes of vibration of postmortem chinchilla TM at: a) 0.776 *kHz*, b) 1.085 *kHz*, c) 3.489 *kHz* and d) 7.675 *kHz*.



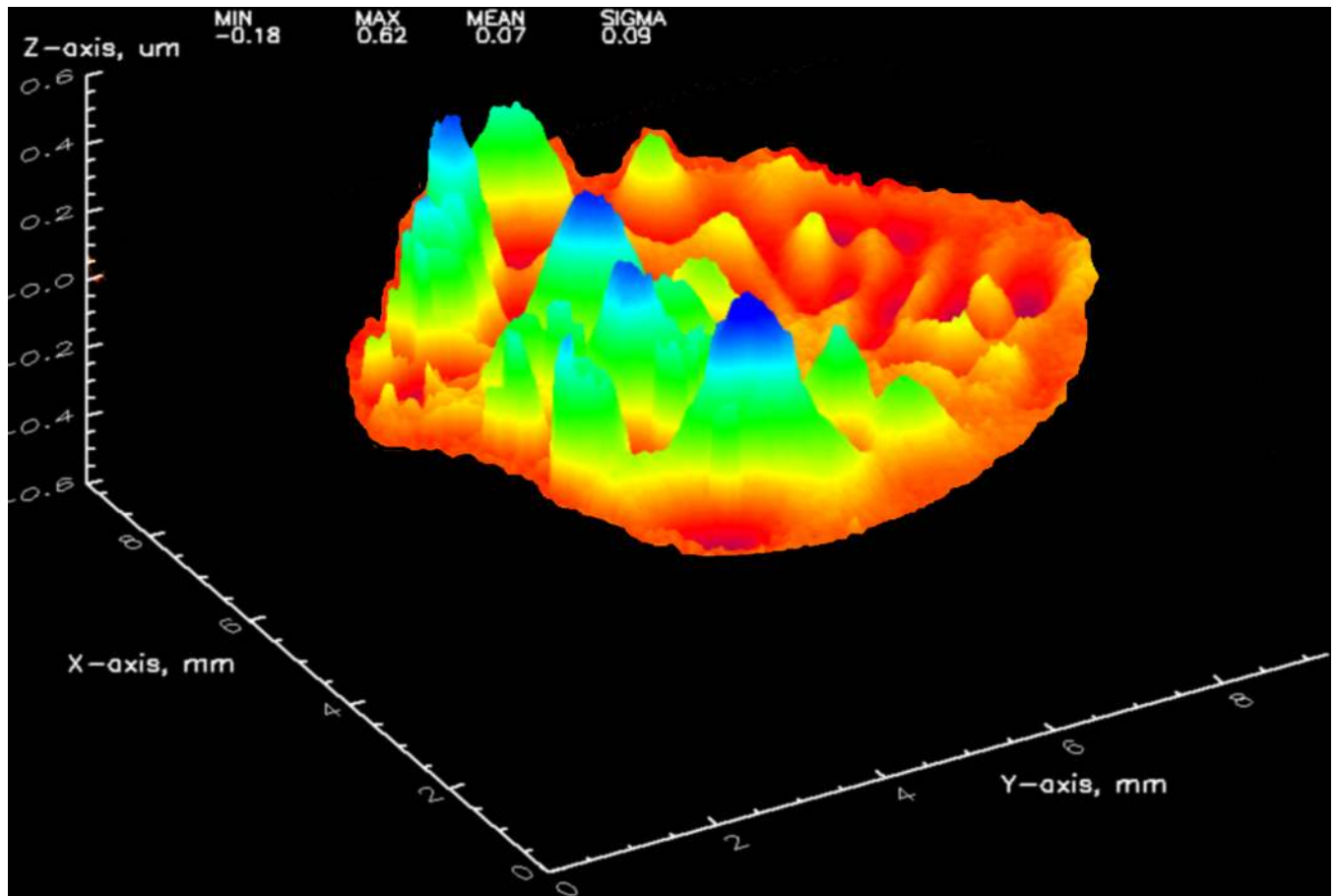


Fig 10.

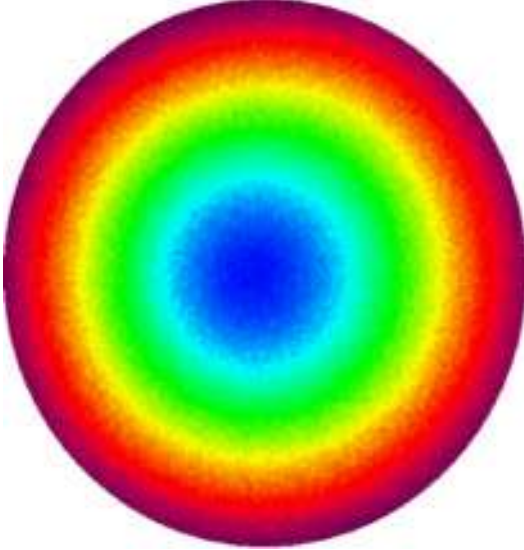
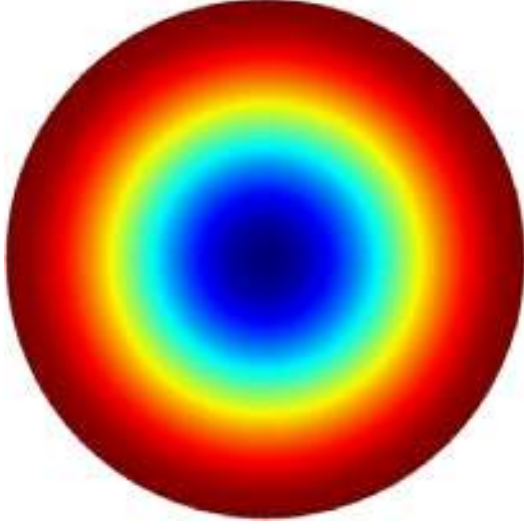
Fig 10a). Wrapped phase map corresponding to the deformations of cadaveric chinchilla TM acoustically excited at the frequency of 3.489 kHz.

Fig 10b). Unwrapped phase map corresponding to the Fig. 10a).

Fig 10c). 3D deformations corresponding to Fig. 9b) showing a peak-to-peak out-of-plane deformation, $d_z = 800 \text{ nm}$.

Table 1

Comparisons between vibration modes of the 110 copper foil alloy membrane sample: experimental results are (EXP), analytical solutions are (AS), and finite element analysis solutions are (FEA). The relative error is computed with respect to the experimental results.

Mode	EXP (Hz)	AS (Hz)	FEA (Hz)	Error (%)		Contour Plot	
				AS	FEA	Experimental	FEA
1	2774	2954	2972	6.09	6.66		
2	6166	6152	6206	0.23	0.64	